

1 **Measurement of tumor antioxidant capacity and prediction of chemotherapy**
2 **resistance in preclinical models of ovarian cancer by positron emission**
3 **tomography**

4 **Authors:**

5 Hannah E. Greenwood¹, Patrick McCormick¹, Thibault Gendron², Matthias Glaser², Raul Pereira¹,
6 Oliver D. K. Maddocks³, Kerstin Sander², Tong Zhang³, Norman Koglin⁴, Mark F. Lythgoe¹, Erik
7 Årstad², Daniel Hochhauser⁵, Timothy H. Witney^{1*}

8
9 **Affiliations:**

10 ¹Centre for Advanced Biomedical Imaging, Division of Medicine, University College London,
11 London, UK

12 ²Institute of Nuclear Medicine and Department of Chemistry, University College London, London,
13 UK

14 ³Wolfson Wohl Cancer Research Centre, Institute of Cancer Sciences, University of Glasgow,
15 Glasgow, UK

16 ⁴Life Molecular Imaging GmbH, Berlin, Germany

17 ⁵Cancer Research UK Drug-DNA Interactions Research Group, UCL Cancer Institute, University
18 College London, London, UK

19

20 *Corresponding Author: Timothy H. Witney (tim.witney@kcl.ac.uk); Tel: +44 (0)20 7188 7188,
21 Ext: 56327; Current address: School of Biomedical Engineering and Imaging Sciences, King's
22 College London, St Thomas' Hospital, London SE1 7EH

1 **Short running title:** Imaging chemotherapy resistance with [¹⁸F]FSPG PET

2

3 **Key words:** [¹⁸F]FSPG, positron emission tomography, xCT, drug resistance, ovarian cancer.

4

5 **Financial Support:** This study was funded through a Wellcome Trust and Royal Society Sir
6 Henry Dale Fellowship (107610/Z/15/Z) and the Cancer Research UK-UCL Centre Development
7 Award (C416/A18088) to Timothy Witney, the CRUK & EPSRC Comprehensive Cancer Imaging
8 Centre at KCL & UCL (C1519/A16463) to Erik Årstad, and financial support from Life Molecular
9 Imaging GmbH (formerly Piramal Imaging) to Timothy Witney. UCL radiochemistry is funded
10 in-part by the Department of Health's NIHR Biomedical Research Centres funding scheme. Oliver
11 Maddocks and Tong Zhang are supported by CRUK Career Development Fellowship
12 C53309/A19702.

13 **Word count:** 4955

14 **Figures:** 6

1 **Translational Relevance**

2 The majority of cancer deaths result from ineffective treatment of metastatic disease. Currently,
3 there is no satisfactory way to identify patients that are refractive to the standard of care. Positron
4 emission tomography (PET) imaging offers a potential solution to this clinical problem through
5 the noninvasive assessment of molecular processes that underpin acquired drug-resistance. The
6 PET radiotracer (4*S*)-4-(3-[¹⁸F]fluoropropyl)-L-glutamate ([¹⁸F]FSPG) provides a surrogate
7 marker of tumor antioxidant capacity through measurement of *de novo* glutathione biosynthesis.
8 Elevated glutathione levels protect tumors from drug-induced oxidative stress, thereby conferring
9 resistance. Here, we show that the magnitude of [¹⁸F]FSPG accumulation in tumors can be used to
10 predict drug resistance and subsequently monitor treatment efficacy in animal models of ovarian
11 cancer. Given that [¹⁸F]FSPG has already been used in pilot clinical trials, identification of drug
12 resistance in patients may enable early intervention, potentially improving disease outcomes.

13

1 **Abstract**

2 **Purpose:** Drug-resistance is a major obstacle for the effective treatment of patients with high grade
3 serous ovarian cancer (HGSOC). Currently, there is no satisfactory way to identify HGSOC
4 patients that are refractive to the standard of care. Here, we propose the system x_c^- radiotracer (4S)-
5 4-(3-[^{18}F]fluoropropyl)-L-glutamate ([^{18}F]FSPG) as a non-invasive method to measure
6 upregulated antioxidant pathways present in drug resistant HGSOC.

7 **Experimental Design:** Using matched chemotherapy sensitive and resistant ovarian cancer cell
8 lines, we assessed their antioxidant capacity and its relation to [^{18}F]FSPG uptake, both in cells and
9 in animal models of human ovarian cancer. We identified the mechanisms driving differential
10 [^{18}F]FSPG cell accumulation and evaluated [^{18}F]FSPG tumor uptake as predictive marker of
11 treatment response in drug-resistant tumors.

12 **Results:** High intracellular glutathione (GSH) and low reactive oxygen species corresponded to
13 decreased [^{18}F]FSPG cell accumulation in drug-resistant *versus* drug-sensitive cells. Decreased
14 [^{18}F]FSPG uptake in drug-resistant cells was a consequence of changes in intracellular cystine, a
15 key precursor in GSH biosynthesis. *In vivo*, [^{18}F]FSPG uptake was decreased ~80% in
16 chemotherapy-resistant A2780 tumors compared to parental drug-sensitive tumors, with non-
17 responding tumors displaying high levels of oxidised-to-reduced GSH. Treatment of drug-resistant
18 A2780 tumors with doxorubicin resulted in no detectable change in tumor volume, GSH or
19 [^{18}F]FSPG uptake.

20 **Conclusions:** This study demonstrates the ability of [^{18}F]FSPG to detect upregulated antioxidant
21 pathways present in drug-resistant cancer. [^{18}F]FSPG may therefore enable the identification of
22 HGSOC patients that are refractory to standard-of-care, allowing the transferral of drug-resistant
23 patients to alternative therapies, thereby improving outcomes in this disease.

1 **Introduction**

2 High-grade serous ovarian cancer (HGSOC) is a devastating disease with a 5-year survival rate of
3 less than 42% (1). Despite initial rates of response to platinum-based chemotherapy of over 80%,
4 the median progression-free survival is just 18 months (2,3). Following first-line treatment,
5 patients frequently relapse with platinum-sensitive disease. However, at each consequent relapse,
6 the probability of response to further platinum-based treatment decreases (4), translating to a
7 progressive decrease in effectiveness of platinum-based drugs. Clinically, response to platinum
8 treatment in ovarian cancer patients is measured as the length of time from treatment to relapse,
9 known as the platinum-free interval (PFI) (5). PFI, however, is a crude measure of drug sensitivity
10 (6) and is particularly poor at predicting response for patients identified as ‘partially-sensitive’.
11 These patients relapse 6-12 months after first line treatment and will all subsequently receive
12 further platinum-based treatment, despite benefit only being appreciable in ~27-33% of cases (7).
13 Better clinically-applicable biomarkers of platinum sensitivity in HGSOC are therefore urgently
14 needed. The ability to identify patients refractive to the standard of care will enable the clinician
15 to select the most appropriate second-line therapy for the individual patient, such as targeted-
16 therapy (e.g. PARP inhibitors), or biologics (e.g. bevacizumab).

17 Biochemical antioxidant mechanisms play a critical role in development of acquired drug-
18 resistance in cancer (8). Antineoplastic agents have been shown to produce oxidative stress in
19 patients who receive these drugs, resulting in cell death in tumors sensitive to treatment (9-17).
20 The plasticity of tumors, however, enables phenotypic adaptation to these oxidizing therapies,
21 frequently mediated through the upregulation of glutathione (GSH), the body’s most abundant
22 antioxidant, in order to preserve cellular redox status and provide defense against reactive

1 oxygen species (ROS) that are produced under conditions of oxidative stress (18). Biopsy
2 samples have shown GSH levels to increase up to 10-fold in ovarian tumors following
3 development of resistance to alkylating agents compared to samples taken before treatment (19).
4 Furthermore, modulators of GSH biosynthesis, such as buthionine sulfoximine (BSO),
5 resensitize human ovarian tumors and cell lines to conventional therapy (20-23), highlighting
6 the importance of GSH in the protection against tumor cell death.

7 One of the key mediators of the cell's antioxidant response is the amino acid transporter system
8 x_c^- , which provides intracellular cysteine for *de novo* GSH biosynthesis. System x_c^- is a sodium
9 independent transporter which under normal physiological conditions permits the exchange of one
10 molecule of extracellular cystine, the dimeric form of cysteine, for one molecule of intracellular
11 glutamate (24). Intracellularly, cystine is rapidly reduced to cysteine, which due to its low
12 intracellular concentration (40–50 μ M) is limiting for GSH synthesis (25). (4S)-4-(3-
13 [18 F]fluoropropyl)-L-glutamate ([18 F]FSPG) is a fluorine-18 labeled glutamate derivative that is
14 specifically transported across the plasma membrane by system x_c^- (26), allowing the non-invasive
15 assessment of system x_c^- transporter activity. Given the overexpression of system x_c^- in a wide-
16 range of tumor types, [18 F]FSPG has been investigated clinically to produce high tumor-to-
17 background PET images in hepatocellular carcinoma (HCC), non-small cell lung cancer and
18 intracranial malignancies (27-29). We have shown previously in preclinical models of HGSOc
19 that [18 F]FSPG uptake is sensitive to an elevation in GSH biosynthesis following drug-induced
20 oxidative stress (30). Given the causal link between the levels of GSH and tumor resistance to
21 therapy, here we examined [18 F]FSPG uptake as a predictive marker of drug resistance in HGSOc
22 prior to treatment and as a marker of response post-therapy.

1 **Materials and methods**

2 *Cell culture*

3 Parental wild-type (WT; 93112519), cisplatin-resistant (CisR; 93112517) and doxorubicin-
4 resistant (DoxR: 93112520) A2780 human ovarian cancer cells (Sigma Aldrich Ltd) were grown
5 in RPMI 1640 media (ThermoFisher Scientific; 21875091) supplemented with 10% foetal bovine
6 serum (ThermoFisher Scientific; 21875091) and 100 U.mL⁻¹ penicillin, 100 µg.mL⁻¹ streptomycin
7 (Sigma Alrich Ltd: P4333). Patient derived PEO1, PEO4 and PEO6 human ovarian cancer cell
8 lines (European Collection of Authenticated Cell Cultures; 10032308, 10032309 and 10032310
9 were cultured as above, supplemented with 10 mM sodium pyruvate (Sigma; S8636). Cells were
10 maintained at 37 °C and 5% CO₂. Clinically-formulated cisplatin (1 µM; TEVA UK Ltd;
11 51642169) or liposomal doxorubicin (0.1 µM; Doxil; Janssen-Cilag Ltd; 668950) was added to
12 the growth media of CisR and DoxR cells, respectively, every third passage. A2780 WT, CisR and
13 DoxR were purchased from an authenticated cell bank and kept within 10 passages of the original
14 vial. Short tandem repeat profiling could not be performed with PEO1, PEO4 or PEO6 cells.
15 Mycoplasma testing was performed on a monthly basis.

16

17 *Drug sensitivity in cell culture*

18 Growth inhibition following drug treatment was characterized using the Vybrant® MTT Cell
19 Proliferation Assay Kit (ThermoFisher Scientific, V13154), according to the manufacturer's
20 instructions. In 96-well plates, A2780 WT, CisR and DoxR cells (2,000 cells/well); and PEO1,
21 PEO4 and PEO6 (5,000 cells/well) were treated with increasing concentrations of clinically-
22 formulated cisplatin or liposomal doxorubicin, 24 h post seeding (0.01 µM to 400 µM). Complete
23 media containing no drug was used as a control. Absorbance was measured at $\lambda = 570$ nm using a

1 Multiskan FC Absorbance Plate Reader (THERMO-LABSYSTEMS). Viable cells were
2 calculated as a percentage of the control group treated with no drug. Dose-response curves were
3 generated and from them half-maximal growth inhibition (EC_{50}) values were determined using
4 GraphPad Prism (sigmoidal dose-response, fixed slope; v.6.0).

5 6 *Clonogenic assay*

7 PEO 1, PEO 4 and PEO 6 cells were seeded in 10 cm dishes at densities of 2×10^3 , 2×10^3 and 1
8 $\times 10^4$ cells in 10 mL media, respectively. 48 h post seeding, cells were treated with clinically-
9 formulated cisplatin (0.02 μ M to 2 μ M) for 72 h. At 72 h drug containing media was replaced with
10 fresh growth media and colonies were left to grow for a further 7 days. Colonies were fixed and
11 stained in 6.0% glutaraldehyde (Sigma, 340355) and 0.5% crystal violet (Sigma, C0775). Colonies
12 which contained >50 cells were counted to determine the surviving fraction (SF) which was
13 calculated by dividing the total number of colonies formed by the number of cells seeded,
14 multiplied by the plating efficiency.

15 16 *Detection of intracellular oxidative stress*

17 ROS were detected in human ovarian cancer cell lines using the cell permeable fluorophore
18 CellROX Orange (Invitrogen, C10443). A2780 WT, CisR and DoxR were seeded in 6-well plates
19 at a density of 5×10^5 cells per well in 2 mL media 24 h prior to performing the assay. PEO 1,
20 PEO 4 and PEO 6 cells were seeded at densities of 2×10^5 , 6×10^5 and 8×10^5 cells per well (2
21 mL media), respectively, 48 h prior to assay to ensure complete cell attachment. Fresh media
22 supplemented with 2 mM glutamine was added to each 6-well plate one hour before the
23 experiment. A final concentration of 1 μ M CellROX Orange reagent was added to each well and

1 incubated for 30 min at 37 °C, protected from light. Cells were then washed with PBS, harvested
2 using 0.05% trypsin-EDTA (Thermo Fisher Scientific; 25300062) and suspended in 1 mL of ice-
3 cold Hanks balanced salt solution (ThermoFisher Scientific; 14025092). The cell suspension was
4 passed through a 35 µM filter and kept on ice prior to analysis on a LSRFortessa™ X-20 flow
5 cytometer (561 nm laser and 586/15 bandpass filter; BD Biosciences), with 20,000 single cell
6 events recorded per sample. Laser power remained constant between matched cell lines but was
7 adjusted for A2780 vs. PEO lines. Data were gated post-acquisition based on forward (FS) and
8 side scattering (SS) profiles to include only single cell events and to exclude cellular debris.

9

10 *Glutamate quantification*

11 The glutamate concentration in cell lysates was determined using a glutamate colorimetric assay
12 kit following the manufactures guidelines (Biovision; K629). Cells were seeded in 6-well plates
13 for glutamate quantification at the densities described above. One hour prior to harvesting the cells,
14 fresh media supplemented with 2 mM glutamine was added to all wells. Following harvesting with
15 trypsin, cells were washed three times with 1 mL of ice-cold PBS. After the final wash, cells were
16 suspended in 200 µL of glutamate assay buffer and sonicated using three sets of five, one-second
17 pulses, on ice. Lysates were then centrifuged at 15,000 × g for 10 min at 4 °C and the supernatant
18 taken for analysis. Total intracellular glutamate was normalized to protein concentration,
19 determined using the Pierce BCA assay (ThermoFisher Scientific; 23225) according to the
20 manufacturer's instructions.

21

22 *Cystine measurements using liquid chromatography-mass spectrometry*

1 Cells seeded in 6-well plates (specific densities stated above) were supplemented with fresh media
2 containing 2 mM glutamine and 200 μ M cystine for one hour. Briefly, following incubation, media
3 samples were removed and diluted into 490 μ L of ice-cold extraction solvent (*v/v* 50% methanol,
4 30% acetonitrile and 20% deionized water). For intracellular cystine quantification, cells were
5 subsequently washed three times with ice cold PBS and lysed in an appropriate volume of ice-cold
6 extraction solvent to ensure $\sim 3 \times 10^6$ cells/mL were collected. Both media samples and cell lysates
7 were centrifuged at $15,000 \times g$ at 1 $^{\circ}$ C for 10 min. The supernatants were subjected to liquid
8 chromatography-mass spectrometry (LC-MS) as previously described (30).

9

10 *In vitro analysis of total GSH*

11 Cells were seeded into 6-well plates as described above. Total GSH was determined using either
12 a colorimetric (Cayman Chemical; 703002) or luminescent (GSH/GSSG-Glo Assay kit, Promega;
13 V6611) assay kit. For luminescent-based GSH quantification, cells were washed in ice-cold PBS,
14 lysed in assay buffer and centrifuged at $15,000 \times g$ at 4 $^{\circ}$ C for 10 min. 5 μ L of supernatant along
15 with 5 μ L of GSH standards (1-100 μ M) were added to white 96-well plates and total GSH
16 determined according to manufacturer's instructions. For colorimetric quantification, cells were
17 processed as above, and total GSH detected according to the manufacturer's guidelines. Total
18 intracellular GSH was normalized to protein concentration.

19

20 *Western blot*

21 Western blot analysis was carried out using an established experimental method (31), adapted for
22 use with the iBind Flex system (ThermoFisher Scientific) for primary and secondary antibody
23 immunoblotting. For cell lysate collection, cells were seeded in 6-well plates, as described above.

1 Rabbit monoclonal antibodies against human xCT (Novus Biologicals; NB300-318), NRF2 (Cell
2 Signaling Technology; 12721), GLS1 (Abcam; ab156876), GCL (Abcam; ab190685; 1:1000
3 dilution), ABCC2 (Cell Signaling Technology; 12559), ABCC6 (Cell Signaling Technology;
4 10666), ABCB1 (Cell Signaling Technology; 13342) and ABCG2 (Cell Signaling Technology;
5 42078) were used for cell lysate analysis. Rabbit anti-human NRF2, GCL, p53 (Cell Signaling
6 Technology; 2527), caspase3 Cell Signaling Technology; 9915) and cleaved-caspase3 antibodies
7 (Cell Signaling Technology; 9915; 1:1000 dilution) were used for tumor lysate evaluation
8 (prepared as described below). Actin was used as a loading control for all experiments (1:1000
9 dilution; Cell Signaling Technology; 4967), with an HRP linked anti-rabbit IgG secondary
10 antibody (1:2000 dilution; Cell Signaling Technology; 7074S).

11

12 *Radiotracer production*

13 Automated radiosynthesis of [¹⁸F]FSPG was accomplished utilizing a Scintomics HBIII platform
14 (Scintomics, Fürstfeldbruck, Germany), according to a previously reported method (30). The
15 decay corrected isolated radiochemical yield was $51 \pm 3\%$ ($n = 6$) after solid phase extraction
16 purification, the radiochemical purity of [¹⁸F]FSPG was $> 98\%$ and the molar activity of the tracer
17 was 4.2-21.9 GBq/ μ mol when starting from 2-4 GBq of [¹⁸F]fluoride. The total synthesis time,
18 from [¹⁸F]fluoride in water to end of reformulation, was approximately 2 h. Clinical-grade
19 [¹⁸F]FDG was obtained from PETNET solutions.

20

21 *Radiotracer uptake in cells*

22 Cells were seeded at the appropriate density in 6-well plates (see above). For all cell uptake
23 experiments, radiotracers were added at a concentration of 0.185 MBq/mL. Cell uptake was

1 performed for 60 min at 37 °C in fresh growth media, following a previously established method
2 (32). Radioactivity in samples was expressed as a percentage of the administered dose per mg
3 protein.

4 5 *In vivo tumor models*

6 All animal experiments were performed in accordance with the United Kingdom Home Office
7 Animal (scientific procedures) Act 1986. 5×10^6 A2780 WT and DoxR cancer cells in 100 μ L
8 Dulbecco's PBS were injected subcutaneously into female Balb/c nu/nu mice aged 6-9 weeks
9 (Charles River Laboratories). Tumor dimensions were measured using an electronic caliper and
10 the volume calculated using the following equation: $\text{volume} = ((\pi/6) \times h \times w \times l)$, where h , w and
11 l represent, height, width and length, respectively. Tumor size was monitored daily and imaging
12 studies took place when tumor volume reached $\sim 100 \text{ mm}^3$.

13 14 *MicroPET imaging studies*

15 Static PET scans were acquired on a Mediso NanoScan PET/CT system (1-5 coincidence mode;
16 3D reconstruction; CT attenuation-corrected; scatter corrected). Mice received a bolus intravenous
17 injection of approximately 3.7 MBq of [^{18}F]FSPG through a tail vein cannula. Following a 40 min
18 uptake period, a 20 min PET scan was acquired. Animals were maintained under isoflurane
19 anesthesia (1.5-2 % in oxygen) at 37 °C during radiotracer administration and throughout the scan.
20 CT images were acquired for anatomical visualization (480 projections; helical acquisition; 50
21 kVp; 300 ms exposure time). Following image reconstruction, (Tera-Tomo 3D; 4 iterations, 6
22 subsets; 0.4 mm isotropic voxel size), VivoQuant software (Invicro) was used to quantify
23 radiotracer uptake. Tumor and hindlimb muscle volumes of interest were constructed from 2D

1 regions drawn manually using the CT image as reference. Data were expressed as percent injected
2 dose per milliliter of tissue (%ID/mL). Tumor-to-background ratios were calculated by dividing
3 the tumor %ID/mL by the muscle %ID/mL.

4

5 *In vivo Doxil treatment studies*

6 For treatment response studies, mice bearing ~100 mm³ size-matched A2780 DoxR tumors were
7 treated by intraperitoneal (i.p.) injection with Doxil (10 mg/kg). A cohort of untreated mice bearing
8 100 mm³ A2780 DoxR tumors were imaged as pre-treatment controls. 24 h post injection (D1),
9 Doxil-treated mice were imaged with [¹⁸F]FSPG PET as described above. A second cohort of mice
10 received a further two Doxil doses, 2 and 5 days after the initial dose. These mice were
11 subsequently imaged with [¹⁸F]FSPG PET 6 days following the initial Doxil treatment (D6).

12

13 *Ex vivo tumor sample preparation*

14 Immediately following sacrifice, tumor tissue was dissected, snap frozen in liquid nitrogen and
15 stored at -80 °C. For GSH and GSSG analysis, each tumor sample was split into two pieces, placed
16 into lysis Matrix tubes containing 1.4 mm ceramic beads (MP Biomedicals; 116913050) and assay
17 buffer (GSH/GSSG-Glo assay, Promega) with or without *N*-ethyl maleimide (NEM; 1 mM),
18 respectively. For Western blot samples, tumor tissue was added to separate Matrix tubes containing
19 1.4 mm ceramic beads and RIPA buffer. Tumor samples were lysed by rapid shaking using a high-
20 speed benchtop reciprocating homogenizer (Fastprep-24™ Sample Preparation Instrument, MP
21 Biomedicals). The lysates were centrifuged at 15,000 × *g* at 4 °C for 10 min and the supernatant
22 collected for analysis. For all *ex vivo* experiments, data were expressed per mg of protein.

23

1 *Statistics*

2 All data were expressed as the mean \pm one standard deviation (SD). Statistical significance was
3 determined using analysis of variance (ANOVA) followed by t-tests multiple comparison
4 correction (Tukey method; GraphPad Prism v.6.0).

5

6

7 **Results**

8 *Cell model characterization*

9 To investigate the role of intracellular redox homeostasis on tumor response to treatment, we used
10 two sets of matched human ovarian cell lines with varying levels of drug sensitivity. The A2780,
11 CisR and DoxR lines were established previously from chronic exposure of the drug-sensitive
12 A2780 WT cells to increasing concentrations of either cisplatin or doxorubicin, respectively
13 (33,34). The cisplatin-sensitive PEO1 cell line was cultured from a patient with relapsed ovarian
14 cancer 22 months after 5-fluorouracil and chlorambucil combination chemotherapy with cisplatin.
15 The PEO4 cisplatin resistant cell line was cultured from ascites taken from the same patient ten
16 months later after further progressive disease but prior to re-treatment with high dose cisplatin.
17 Finally, the PEO6 cell line was obtained from ascites a further three months later, after the patient
18 failed to respond to high-dose cisplatin (35).

19

20 We initially verified drug response rates of the matched A2780 cell lines in culture. CisR cells
21 displayed moderate sensitivity to cisplatin in comparison to WT cells, with an EC₅₀ of 10.1 μ M \pm
22 0.3 μ M *versus* 0.8 μ M \pm 0.2 μ M, respectively ($n = 3$; $P < 0.0001$; **Fig. 1A**), confirming previously-
23 reported values (36). DoxR cells were resistant to prolonged exposure at high micromolar

1 doxorubicin concentrations ($EC_{50} = 29 \mu\text{M} \pm 2.1 \mu\text{M}$ and $0.47 \mu\text{M} \pm 0.03 \mu\text{M}$ for DoxR and WT,
2 respectively; $n = 3$; $P < 0.0001$; **Fig. 1B**), again confirming previous findings (36). Interestingly,
3 CisR and DoxR cells were cross-resistant to doxorubicin and cisplatin, respectively, despite not
4 having been exposed to these drugs – possibly highlighting a shared mechanism of resistance. The
5 EC_{50} for cisplatin in PEO1 cells was $2.6 \mu\text{M} \pm 0.85 \mu\text{M}$, with PEO4 cells exhibiting lowered
6 sensitivity to cisplatin in comparison to PEO1 cells, with an EC_{50} value of $14 \mu\text{M} \pm 5.3 \mu\text{M}$ ($n =$
7 3 ; $P = 0.01$; Fig 1C). There was no significant difference in EC_{50} between PEO1 and PEO6 cells
8 ($n = 3$; $P = 0.083$). However, the dose required to kill 90% of the cells was 3-fold higher for PEO6
9 ($19 \mu\text{M} \pm 4.8 \mu\text{M}$ for PEO1 vs. $66 \mu\text{M} \pm 35 \mu\text{M}$ for PEO6; $n = 3$; $P = 0.04$), revealing a small
10 subset of PEO6 cells to be highly resistant. Motivated by this, a clonogenic assay was used to
11 further explore cisplatin resistance in these cell lines. PEO6 cell lines showed decreased sensitivity
12 to $0.5 \mu\text{M}$ cisplatin following treatment compared to PEO1 cells ($SF = 0.78 \pm 0.22$ vs. $0.432 \pm$
13 0.02 , $P = 0.04$, $n = 3$), with both PEO4 and PEO6 cell lines exhibiting improved survival following
14 treatment with $2 \mu\text{M}$ cisplatin ($SF = 0.08 \pm 0.04$, 0.12 ± 0.04 and 0.005 ± 0.004 for PEO4, PEO6
15 and PEO1, respectively; $n = 3$; $P = 0.05$, PEO1 vs PEO4; $P = 0.008$, PEO1 vs. PEO 6;
16 **Supplemental Fig. S1**).

17

18 *Drug-resistant ovarian cancer cells upregulate antioxidant defense mechanisms*

19 We hypothesized that drug resistance in these cell lines was mediated, at least in-part, by the
20 upregulation of key antioxidant pathways. In support of this hypothesis, we found that basal
21 intracellular ROS levels were decreased 24% in CisR ($P = 0.03$) and 86% in DoxR cells ($P <$
22 0.0001), compared to the WT parental cells ($n = 3$; **Fig. 1D**). Intracellular ROS in the PEO4 and
23 PEO6 cell lines were also decreased 60% ($P = 0.02$) and 55% ($P = 0.03$), respectively, compared

1 to PEO1 ($n = 4$; **Fig. 1E**). Accompanying this decrease in intracellular ROS, intracellular GSH
2 was increased 1.8-fold in the CisR cells and 3.3-fold in DoxR cells, compared to WT cells ($n = 3$;
3 $P = 0.04$, WT vs. CisR; and 0.0002, WT vs. DoxR; **Fig. 1F**), with GSH increased 2.7- and 3.8-fold
4 in the PEO4 and PEO6 cells compared to PEO1 ($n = 3$; $P < 0.0001$, PEO1 vs. PEO4; and $P <$
5 0.0001 , PEO1 vs. PEO6; **Fig. 1G**).

6

7 *[¹⁸F]FSPG, but not [¹⁸F]FDG uptake predicts drug sensitivity in A2780 cells*

8 We have previously shown that system x_c^- provides a functional readout of *de novo* GSH
9 biosynthetic flux, which can be imaged non-invasively using [¹⁸F]FSPG PET (30). Given that the
10 rate of GSH biosynthesis may provide a surrogate marker of drug sensitivity, we next assessed
11 system x_c^- -mediated [¹⁸F]FSPG uptake in drug-sensitive and drug-resistant ovarian tumor cells in
12 culture. The molecular structure of [¹⁸F]FSPG is shown in **Fig 2A**. In CisR cells, [¹⁸F]FSPG
13 accumulation was reduced by 57% compared to WT, falling from 9.9 ± 1.1 % radioactivity/mg
14 protein to 4.3 ± 0.3 % radioactivity/mg protein ($P < 0.0001$). In the more resistant DoxR cells,
15 [¹⁸F]FSPG accumulation was 81% lower than WT (1.6 ± 0.1 % radioactivity/mg protein; $n = 4$; P
16 < 0.0001 ; **Fig. 2B**). [¹⁸F]FDG is routinely used in the clinic for cancer diagnosis and staging. In
17 contrast to [¹⁸F]FSPG, there was no correlation between [¹⁸F]FDG uptake and the magnitude of
18 drug resistance (Supplemental **Fig. S2**), with [¹⁸F]FDG cell uptake measured at 1.5 ± 0.2 %
19 radioactivity/mg protein, 10.6 ± 2.1 % radioactivity/mg protein and 6.3 ± 1.1 % radioactivity/mg
20 protein, for CisR, DoxR and WT, respectively ($n = 3$). Confirming findings in the A2780 cell lines,
21 [¹⁸F]FSPG uptake was decreased 29 % and 41 % in the more resistant PEO4 and PEO6 cell lines,
22 compared to PEO1 cells (2.5 ± 0.3 % radioactivity/mg protein, 1.8 ± 0.2 % radioactivity/mg protein

1 and 1.5 ± 0.3 % radioactivity/mg protein, for PEO1, PEO4 and PEO6, respectively; ($n = 3-4$; $P =$
2 0.03 , PEO1 vs PEO4; and $P = 0.003$, PEO1 vs PEO6; **Fig. 2C**).

3

4 *Intracellular cystine is decreased in chemotherapy resistant cells*

5 System x_c^- is the key transporter used in tumor cells for the exchange of intracellular glutamate
6 with extracellular cystine (**Fig. 3A**). The altered radiotracer flux through system x_c^- occurred in the
7 absence of any changes in xCT protein expression, the transporter component of system x_c^- . Splice
8 variants of glutaminase 1, the kidney-type glutaminase (KGA) isoform and the glutaminase C
9 isoform (GAC), which provide intracellular glutamate through glutaminolysis, showed elevated
10 expression in the CisR and DoxR resistant lines in comparison to WT (**Fig. 3B**). The PEO4 and
11 PEO6 cell lines showed increased expression of the redox-sensitive transcription factor NRF2 and
12 one of its downstream targets glutamate-cysteine ligase (GCL) – the rate limiting enzyme in GSH
13 biosynthesis (**Fig. 3B**).

14 The absence of changes in [^{18}F]FSPG transporter expression motivated us to investigate the roles
15 of intracellular concentrations of glutamate and cystine to determine their potential role in
16 [^{18}F]FSPG retention. In the A2780 cell lines, there was no significant difference in the intracellular
17 concentration of glutamate, despite the observed differences in glutaminase expression ($n = 3$; P
18 > 0.05 ; **Fig. 3C**). Intracellular cystine however was decreased over 90% in the drug resistant
19 A2780 lines, compared to drug-sensitive ($n = 3$; $P = 0.0019$, WT vs. CisR; and $P = 0.0021$, WT
20 vs. DoxR); **Fig. 3F**). Markedly lower intracellular cystine was also measured in PEO4 and PEO6
21 cells compared to PEO1s (86% and 65% decrease, respectively; $n = 3$; $P = 0.018$, PEO1 vs. PEO4;
22 and $P = 0.059$, PEO1 vs. PEO6; **Fig. 3F**). Additionally, in the PEO cell lines, there was a 54%

1 decrease in intracellular glutamate for PEO4 cells and 40% in the PEO6 cells, compared to PEO1
2 ($n = 3$; $P = 0.005$, PEO1 vs. PEO4; and $P = 0.02$, PEO1 vs. PEO6; **Fig. 3D**).

3

4 *ABC transporter expression*

5 ATP-binding cassette (ABC) transporter proteins play an important role in acquired drug
6 resistance, facilitating the efflux of anticancer drugs, frequently as GSH-conjugates (37). To
7 explore the role of key ABC transporters and their potential link to the tumor antioxidant response,
8 we examined their expression in our panel of ovarian cancer cells. In the DoxR cells, ABCB1 and
9 ABCC2 was expressed to high levels, whereas functional expression of these transporters was
10 absent in the WT and CisR lines. Conversely, ABCG2 expression was elevated in WT cells, with
11 no expression observed in all other lines. The ABCC6 transporter was not expressed in any of the
12 cell lines tested, with PEO1, PEO4 and PEO6 cells expressing neither ABCB1, ABCC2, ABCG2
13 nor ABCC6 (Supplemental **Fig. S3**).

14

15 *[¹⁸F]FSPG uptake can differentiate chemotherapy sensitive and resistant tumors in vivo*

16 We next evaluated the specificity of [¹⁸F]FSPG to non-invasively detect drug resistance in living
17 subjects using small animal PET. [¹⁸F]FSPG distribution was characterized by high uptake in WT
18 tumors 40-60 min post injection. Conversely, low tumor-associated radioactivity was measured in
19 size-matched DoxR tumors. Representative static [¹⁸F]FSPG maximum-intensity projections
20 (MIPs) are shown in **Fig. 4A**, with single-slice images are displayed in **Supplementary Fig. S4**,
21 and the corresponding three-dimensional (3D) movies displayed as movies **S1** and **S2**.
22 Quantification of image-derived [¹⁸F]FSPG uptake revealed a 79% decrease in [¹⁸F]FSPG uptake
23 in DoxR tumors compared to WT tumors (7.9 ± 0.7 %ID/mL vs. 1.7 ± 0.4 %ID/mL; $n = 5-6$

1 animals/group; $P < 0.0001$; **Fig. 4B**). [^{18}F]FSPG tumor retention was above background tissue
2 uptake for both drug sensitive and drug resistant tumors, with tumor-to-muscle ratios of 18.8 ± 5.2
3 and 2.7 ± 1.6 for WT and DoxR, respectively ($n = 5-6$ animals/group; $P < 0.0001$; **Supplementary**
4 **Fig. S5**). To understand redox alterations that may underpin this differential [^{18}F]FSPG uptake,
5 the levels of GSH and GSSG were evaluated in snap-frozen tumor samples. In DoxR tumors, GSH
6 was increased 1.6-fold compared to WT, with a ~ 20 -fold increase in the ratio of GSSG to GSH
7 measured in the drug-resistant tumors ($n = 3$; $P = 0.0002$; **Fig. 4C**). Western blot analysis revealed
8 xCT, NRF2, GCLC and glutaminase protein expression remained unchanged between the sensitive
9 and resistant tumors. However, a stabilization in p53 expression was observed in the DoxR tumor
10 samples (**Fig. 4D**). PEO1, PEO4 and PEO6 cells failed to grow *in vivo*, meaning that we were
11 unable to further corroborate our findings in cell culture using this model.

12

13 *[^{18}F]FSPG uptake is unchanged in DoxR tumors following therapy*

14 We have shown previously that [^{18}F]FSPG is an early and sensitive marker of drug-induced
15 oxidative stress in A2780 WT tumors (30). To further explore [^{18}F]FSPG as a robust marker of
16 both drug response and treatment failure, we assessed [^{18}F]FSPG uptake in DoxR tumor xenografts
17 over the same 6-day Doxil treatment time course (**Fig. 5A**). Representative [^{18}F]FSPG MIPs are
18 shown in **Fig. 5B**, with single-slice images illustrated in **Supplementary Fig. S6**, and
19 corresponding 3D movies displayed as movies **S3**, **S4** and **S5**. Unlike in the A2780 WT tumors
20 (30), there was no significant difference in [^{18}F]FSPG tumor uptake between animals imaged on
21 D0, D1 and D6 (1.8 ± 0.4 %ID/mL, 1.9 ± 0.4 %ID/mL and 1.7 ± 0.6 %ID/mL, respectively; $n =$
22 $5-6$ animals/group; $P = 0.94$, D0 vs. D1; and $P = 0.9$, D0 vs. D6; **Fig. 5C**). Over the course of the
23 experiment, there was also no significant difference in tumor size measured between treated and

1 untreated animals (**Fig. 5D**), indicating failure of this treatment regimen. Supporting these
2 findings, there was no change in tumor GSH, GSSG:GSH ratio (**Fig. 5E and F**), markers of
3 oxidative stress (NRF2) or levels of apoptosis following treatment, shown through measurements
4 of caspase 3 cleavage (**Fig. 5G**).

5
6

7 **Discussion**

8 Chemotherapy agents are extensively used for the treatment of many cancers, with the aim to target
9 rapidly-growing tissue, often through DNA damage, growth arrest and the induction of cell death
10 (38). The low therapeutic index of antineoplastic drugs, however, means that relatively small
11 changes in the sensitivity of tumor cells to these agents can be detrimental to patient outcome. The
12 development of novel imaging methods to monitor drug-induced cell death as an indicator of drug
13 efficacy have shown great promise, potentially allowing for a timely intervention following the
14 emergence of drug resistance (39-43). Monitoring response post-treatment, however, is often
15 hampered by difficulties predicting the timescale of response in individual patients. Furthermore,
16 the effective clearance of dying tumor cells by the innate immune system and the high cell turnover
17 in untreated tumors results in cell death being a temporally unstable biomarker of response (44).

18

19 The adaptations that occur in cancer cells as a consequence of acquired drug resistance provide
20 ample opportunity for the development of novel, targeted PET radiotracers that have the potential
21 to predict response *prior* to therapy. Here, we used the redox-sensitive radiotracer, [¹⁸F]FSPG, as
22 a surrogate marker of drug resistance. Drug resistant cancer cells have the ability to maintain a
23 highly reduced intracellular environment to protect themselves from the harmful effects of

1 oxidative stress, thereby conferring treatment resistance (45-47). Using matched drug-sensitive
2 and drug-resistant ovarian cancer cells, we showed that resistance to either cisplatin or doxorubicin
3 corresponded with an increase in tumor antioxidant capacity, defined through the elevation of
4 intracellular GSH and a decrease in ROS. A key component of the tumor's antioxidant system is
5 system x_c^- , which provides cystine for *de novo* GSH biosynthesis. Differential x_c^- activity in drug-
6 resistant *versus* sensitive A2780 and PEO cells was quantified through measurements of
7 [^{18}F]FSPG cell accumulation, which occurred in the absence of changes in transporter expression.
8 In drug-sensitive cells, [^{18}F]FSPG accumulated to high levels, whereas low intracellular levels
9 were observed in cells resistant to therapy. In comparison, baseline glucose utilization, shown
10 through [^{18}F]FDG uptake, was a poor predictive marker of response.

11
12 We have previously shown that the intracellular concentrations of system x_c^- substrates glutamate
13 and cystine mediate [^{18}F]FSPG uptake and retention in A2780 WT tumors (30). In addition, drug-
14 induced oxidative stress in these tumor cells resulted in rapid depletion of intracellular cystine as
15 a consequence of an increase in the rate of *de novo* GSH biosynthesis, which could be imaged by
16 [^{18}F]FSPG PET (30). In all drug-resistant cell lines examined here, intracellular cystine
17 concentrations were substantially decreased compared to drug-sensitive lines, corresponding to
18 large increases in steady-state GSH. In the drug-resistant PEO4 and PEO6 cell lines, where
19 intracellular GSH concentrations were highest of all the cell lines examined, intracellular
20 glutamate – another biosynthetic precursor of GSH – was also significantly decreased compared
21 to the drug-sensitive PEO1 cells. Lowered intracellular glutamate was not observed in the drug-
22 resistant A2780 cell lines which expressed elevated levels of GLS1, a key metabolic enzyme that
23 catalyzes the conversion of glutamine to glutamate. Through increased glutaminolysis, it is thought

1 that drug-resistant A2780 cells maintained high intracellular glutamate concentrations despite
2 elevated flux into GSH. Conversely, this compensatory mechanism was absent in the resistant
3 PEO4 and PEO6 cell lines which did not upregulate GLS1, which may account for the reduction
4 in intracellular glutamate when compared to PEO1 cells. The PEO4 and PEO6 cell lines did
5 however upregulate the expression of the redox-sensitive transcription factor NRF2 which
6 paralleled elevated GCL, its downstream target and the rate limiting enzyme in GSH biosynthesis.
7 These data suggest there are multiple mechanisms at play that result in elevated *de novo* GSH
8 biosynthesis and consequent cystine consumption in drug-resistant cells.

9
10 Low levels of intracellular cystine present in drug-resistant cells accompanied decreased
11 [¹⁸F]FSPG retention compared to their parental drug-sensitive cell line. This decrease in [¹⁸F]FSPG
12 accumulation can be understood by considering the mechanism of system x_c⁻ transport. System x_c⁻
13 activity is mediated by the membrane concentration gradients of both glutamate (high intracellular,
14 low extracellular) and cystine (low intracellular, high extracellular) (48). Depletion of intracellular
15 cystine acts to increase system x_c⁻-mediated cystine uptake into the cell, with a corresponding
16 increase in glutamate efflux. As [¹⁸F]FSPG can replace glutamate as an exchange partner with
17 cystine, lowered intracellular [¹⁸F]FSPG measured in drug resistant tumors may be a consequence
18 of elevated radiotracer efflux from the cell. Additionally, increased cystine uptake may
19 alternatively lead to higher occupancy of the transporter by the natural substrate and therefore
20 lower [¹⁸F]FSPG uptake. Furthermore, a decrease in intracellular glutamate, as observed in PEO4
21 and PEO6 cells, will lower the rate of glutamate efflux, thereby reducing the rate of both cystine
22 and [¹⁸F]FSPG uptake. Taken together, a depletion of either intracellular glutamate or cystine is
23 predicted to reduce overall [¹⁸F]FSPG accumulation, as shown in this study. A schematic

1 illustrating the putative relationship between the intracellular-to-extracellular concentration
2 gradients of cystine and glutamate, [^{18}F]FSPG tumor retention, and drug resistance is shown in
3 **Fig. 6.**

4
5 Corroborating our findings in culture, tumor-associated [^{18}F]FSPG was decreased in drug-resistant
6 A2780 DoxR xenografts when compared to drug-sensitive WT tumors, which was also
7 independent of any changes in xCT expression. In the drug-resistant DoxR tumors, we observed
8 an elevation in total tumor GSH and 21-fold increase in GSSG:GSH ratio when compared to WT
9 – indicating an adaptive mechanism to maintain a decreased intracellular environment through
10 upregulation of this key antioxidant pathway. This reducing environment facilitates the protection
11 against ROS-induced cell death, subsequently lowering drug induced toxicity and resulting in
12 drug-resistance. We have previously shown that [^{18}F]FSPG uptake is an early and sensitive marker
13 of treatment response in doxorubicin-sensitive A2780 WT tumors (30). WT tumors were treated
14 with Doxil over the same 6 day treatment time course described here (Fig. 5A), with [^{18}F]FSPG
15 retention decreased by a significant 42% 24h post therapy. In these drug-sensitive WT tumors a
16 reduction in [^{18}F]FSPG coincided with a depletion in tumor GSH but occurred prior to measurable
17 changes in tumor volume, which became evident 4 days after the initial round of treatment (30).
18 Given that DoxR tumors upregulate the antioxidant GSH and maintain low levels of ROS, we
19 asked if this reducing environment was sufficient to protect these tumors from oxidizing Doxil
20 treatment and whether [^{18}F]FSPG PET could monitor drug response (or its absence) post therapy.
21 In these resistant tumors, three doses of Doxil therapy over the 6-day treatment time course did
22 not induce caspase 3 activation, with treatment unable to alter tumor growth *in vivo*. Treatment
23 failure corresponded with an absence of changes in total GSH and the GSSG:GSH ratio from

1 baseline. Importantly, no differences in [¹⁸F]FSPG tumor uptake were measured between treatment
2 groups, indicating that [¹⁸F]FSPG uptake can not only be used to predict drug resistance, but
3 monitor treatment response, and indeed treatment failure.

4
5 The non-invasive imaging of chemotherapy-resistant xenografts with [¹⁸F]FSPG holds some
6 limitations. The tumoral heterogeneity in human ovarian cancer results in multiple highly complex
7 mechanisms of chemotherapy resistance, as previously reported (49,50). We have shown here that
8 [¹⁸F]FSPG can be used as a non-invasive method to identify chemotherapy-resistance tumors
9 through measurement of their antioxidant capacity. Other well-established mechanisms of
10 resistance include the upregulation of the ABC efflux pumps (37). In the cell lines tested here,
11 there was no clear pattern of ABC transporter upregulation in the drug-resistant cells, with only
12 A2780 DoxR cells expressing detectable levels of ABCB1 and ABCC2. In DoxR cells, elevated
13 GSH observed (**Fig. 1F**) may be a requirement for ABC transporter-mediated efflux of
14 doxorubicin-GSH conjugates. Upregulation of *de novo* GSH synthesis as a consequence of ABC
15 transporter expression could presumably affect intracellular cystine levels and therefore reduce
16 [¹⁸F]FSPG retention. From this current study, however, it is unclear whether the detection of
17 resistant tumors using mechanisms to overcome insult with chemotherapeutic drugs that do not
18 cause changes in the cellular antioxidant response will cause a change in tumor [¹⁸F]FSPG uptake.
19 Moreover, it is expected that metabolic adaptation in tumors, such as altered anaplerotic flux, may
20 alter [¹⁸F]FSPG uptake irrespective of the resistance-status of the cells. Regarding clinical utility,
21 it may therefore be necessary to acquire a baseline scan for each patient upon diagnosis, with
22 follow-up [¹⁸F]FSPG scans performed upon relapse. Importantly, however, as [¹⁸F]FSPG has

1 already been examined in human clinical trials, there are few barriers to the use of [¹⁸F]FSPG as a
2 predictive marker of drug resistance in patients.

3

4 **Conclusion**

5 Here, we have shown that [¹⁸F]FSPG uptake is uniquely sensitive to the upregulated antioxidant
6 pathways present in drug-resistant human ovarian tumors. In the drug-resistant lines, low
7 [¹⁸F]FSPG uptake corresponded with decreased ROS and higher baseline GSH concentrations in
8 comparison to drug-sensitive tumors. [¹⁸F]FSPG may therefore enable the identification of ovarian
9 cancer patients that are refractory to the standard of care, as well as monitor their response post-
10 treatment. Transferal of drug-resistant patients to alternative therapies has the potential to increase
11 tumor response and patient survival. In addition, [¹⁸F]FSPG PET holds great potential for the
12 prediction of drug sensitivity in a range of other malignancies that share the same underlying
13 mechanisms of resistance.

14

15 **Acknowledgments**

16 The authors would like to thank Stephen Patrick, May Zaw-Thin and Andrew Stephens for
17 insightful scientific discussions and William Day for help with flow cytometric experiments.

18

1 **References**

- 2 1. 2012 Ovarian cancer statistics In Cancer Research UK.
3 <[http://www.cancerresearchuk.org/health-professional/cancer-statistics/statistics-by-](http://www.cancerresearchuk.org/health-professional/cancer-statistics/statistics-by-cancer-type/ovarian-cancer/survival#heading-Zero)
4 [cancer-type/ovarian-cancer/survival#heading-Zero](http://www.cancerresearchuk.org/health-professional/cancer-statistics/statistics-by-cancer-type/ovarian-cancer/survival#heading-Zero)>.
- 5 2. Chen M, Jin Y, Bi Y, Yin J, Wang Y, Pan L. A survival analysis comparing women with
6 ovarian low-grade serous carcinoma to those with high-grade histology. *Oncotargets Ther*
7 **2014**;7:1891-9.
- 8 3. Wiedemeyer WR, Beach JA, Karlan BY. Reversing Platinum Resistance in High-Grade
9 Serous Ovarian Carcinoma: Targeting BRCA and the Homologous Recombination
10 System. *Front Oncol* **2014**;4:34.
- 11 4. Parmar MKB, Ledermann JA, Colombo N, du Bois A, Delaloye JF, Kristensen GB, *et al.*
12 Paclitaxel plus platinum-based chemotherapy versus conventional platinum-based
13 chemotherapy in women with relapsed ovarian cancer: the ICON4/AGO-OVAR-2.2 trial.
14 *Lancet* **2003**;361(9375):2099-106.
- 15 5. Pujade-Lauraine E, Alexandre J. Update of randomized trials in recurrent disease. *Ann*
16 *Oncol* **2011**;22 Suppl 8:viii61-viii4.
- 17 6. Markman M RR, Hakes T, Reichman B, Hoskins W, Rubin S, Jones W, Almadrones L,
18 Lewis JL Jr. Second-line platinum therapy in patients with ovarian cancer previously
19 treated with cisplatin. *J Clin Oncol* **1991**;9(3):389-93.
- 20 7. Colombo N, Gore M. Treatment of recurrent ovarian cancer relapsing 6–12 months post
21 platinum-based chemotherapy. *Crit Rev Oncol Hemat* **2007**;64(2):129-38.
- 22 8. Mullany LK, Richards JS. Minireview: animal models and mechanisms of ovarian cancer
23 development. *Endocrinology* **2012**;153(4):1585-92.
- 24 9. Clemens MR, Ladner C, Ehniger G, Einsele H, Renn W, Buhler E, *et al.* Plasma vitamin
25 E and beta-carotene concentrations during radiochemotherapy preceding bone marrow
26 transplantation. *Am J Clin Nutr* **1990**;51(2):216-9.
- 27 10. Durken M, Agbenu J, Finckh B, Hubner C, Pichlmeier U, Zeller W, *et al.* Deteriorating
28 free radical-trapping capacity and antioxidant status in plasma during bone marrow
29 transplantation. *Bone Marrow Transpl* **1995**;15(5):757-62.

- 1 11. Erhola M, Kellokumpu-Lehtinen P, Metsa-Ketela T, Alanko K, Nieminen MM. Effects of
2 anthracyclin-based chemotherapy on total plasma antioxidant capacity in small cell lung
3 cancer patients. *Free Radic Biol Med* **1996**;21(3):383-90.
- 4 12. Faber M, Coudray C, Hida H, Mousseau M, Favier A. Lipid peroxidation products, and
5 vitamin and trace element status in patients with cancer before and after chemotherapy,
6 including adriamycin. A preliminary study. *Biol Trace Elem Res* **1995**;47(1-3):117-23.
- 7 13. Faure H, Coudray C, Mousseau M, Ducros V, Douki T, Bianchini F, *et al.* 5-
8 Hydroxymethyluracil excretion, plasma TBARS and plasma antioxidant vitamins in
9 adriamycin-treated patients. *Free Radic Biol Med* **1996**;20(7):979-83.
- 10 14. Ladner C, Ehninger G, Gey KF, Clemens MR. Effect of etoposide (VP16-213) on lipid
11 peroxidation and antioxidant status in a high-dose radiochemotherapy regimen. *Cancer*
12 *Chemother Pharmacol* **1989**;25(3):210-2.
- 13 15. Look MP, Musch E. Lipid peroxides in the polychemotherapy of cancer patients.
14 *Chemotherapy* **1994**;40(1):8-15.
- 15 16. Sangeetha P, Das UN, Koratkar R, Suryaprabha P. Increase in free radical generation and
16 lipid peroxidation following chemotherapy in patients with cancer. *Free Radic Biol Med*
17 **1990**;8(1):15-9.
- 18 17. Weijl NI, Hopman GD, Wipkink-Bakker A, Lentjes EG, Berger HM, Cleton FJ, *et al.*
19 Cisplatin combination chemotherapy induces a fall in plasma antioxidants of cancer
20 patients. *Ann Oncol* **1998**;9(12):1331-7.
- 21 18. Balendiran GK, Dabur R, Fraser D. The role of glutathione in cancer. *Cell Biochem Funct*
22 **2004**;22(6):343-52.
- 23 19. Britten RA, Green JA, Warenius HM. Cellular glutathione (GSH) and glutathione S-
24 transferase (GST) activity in human ovarian tumor biopsies following exposure to
25 alkylating agents. *Int J Radiat Oncol Biol Phys* **1992**;24(3):527-31.
- 26 20. Calvert P, Yao K-S, Hamilton TC, O'Dwyer PJ. Clinical studies of reversal of drug
27 resistance based on glutathione. *Chem-Biol Interact* **1998**;111-112:213-24.
- 28 21. Lewis AD, Duran GE, Lau DH, Sikic BI. Sensitization of drug resistant human ovarian
29 cancer cells to cyanomorpholino doxorubicin (MRA-CN) by modulation of glutathione
30 metabolism. *Int J Radiat Oncol Biol Phys* **1992**;22(4):821-4.
- 31 22. Ozols RF, Louie KG, Plowman J, Behrens BC, Fine RL, Dykes D, *et al.* Enhanced
32 melphalan cytotoxicity in human ovarian cancer in vitro and in tumor-bearing nude mice

- 1 by buthionine sulfoximine depletion of glutathione. *Biochem Pharmacol* **1987**;36(1):147-
2 53.
- 3 23. Pan B, Yao KS, Monia BP, Dean NM, McKay RA, Hamilton TC, *et al.* Reversal of
4 cisplatin resistance in human ovarian cancer cell lines by a c-jun antisense
5 oligodeoxynucleotide (ISIS 10582): evidence for the role of transcription factor
6 overexpression in determining resistant phenotype. *Biochem Pharmacol* **2002**;63(9):1699-
7 707.
- 8 24. Bridges RJ, Natale NR, Patel SA. System x(c)(-) cystine/glutamate antiporter: an update
9 on molecular pharmacology and roles within the CNS. *Br J of Pharmacol* **2012**;165(1):20-
10 34.
- 11 25. Tian M, Guo F, Sun Y, Zhang W, Miao F, Liu Y, *et al.* A fluorescent probe for intracellular
12 cysteine overcoming the interference by glutathione. *Org Biomol Chem* **2014**;12(32):6128-
13 33.
- 14 26. Koglin N, Mueller A, Berndt M, Schmitt-Willich H, Toschi L, Stephens AW, *et al.* Specific
15 PET Imaging of xc- Transporter Activity Using a 18F-Labeled Glutamate Derivative
16 Reveals a Dominant Pathway in Tumor Metabolism. *Clin Cancer Res* **2011**;17(18):6000-
17 11.
- 18 27. Mitra ES, Koglin N, Mosci C, Kumar M, Hoehne A, Keu KV, *et al.* Pilot Preclinical and
19 Clinical Evaluation of (4S)-4-(3-[18F]Fluoropropyl)-L-Glutamate (18F-FSPG) for
20 PET/CT Imaging of Intracranial Malignancies. *PLoS One* **2016**;11(2):e0148628.
- 21 28. Baek S, Choi CM, Ahn SH, Lee JW, Gong G, Ryu JS, *et al.* Exploratory clinical trial of
22 (4S)-4-(3-[18F]fluoropropyl)-L-glutamate for imaging xC- transporter using positron
23 emission tomography in patients with non-small cell lung or breast cancer. *Clin Cancer*
24 *Res* **2012**;18(19):5427-37.
- 25 29. Kavanaugh G, Williams J, Morris AS, Nickels ML, Walker R, Koglin N, *et al.* Utility of
26 [18F]FSPG PET to Image Hepatocellular Carcinoma: First Clinical Evaluation in a US
27 Population. *Mol Imaging Biol* **2016**;18(6):924-34.
- 28 30. McCormick PN, Greenwood HE, Glaser M, Maddocks ODK, Gendron T Sander K, *et al.*
29 Assessment of tumor redox status through (S)-4-(3-[18F]fluoropropyl)-L-glutamic acid
30 positron emission tomography imaging of system xc- activity. *Cancer Res* **2018** doi
31 10.1158/0008-5472.CAN-18-2634.
- 32 31. Witney TH, Kettunen MI, Day SE, Hu D-e, Neves AA, Gallagher FA, *et al.* A Comparison
33 between Radiolabeled Fluorodeoxyglucose Uptake and Hyperpolarized 13C-Labeled
34 Pyruvate Utilization as Methods for Detecting Tumor Response to Treatment. *Neoplasia*
35 **2009**;11(6):574-582.

- 1 32. Witney TH, James ML, Shen B, Chang E, Pohling C, Arksey N, *et al.* PET imaging of
2 tumor glycolysis downstream of hexokinase through noninvasive measurement of pyruvate
3 kinase M2. *Sci Transl Med* **2015**;7(310):310ra169-310ra169.
- 4 33. Louie KG, Behrens BC, Kinsella TJ, Hamilton TC, Grotzinger KR, McKoy WM, *et al.*
5 Radiation Survival Parameters of Antineoplastic Drug-sensitive and -resistant Human
6 Ovarian Cancer Cell Lines and Their Modification by Buthionine Sulfoximine. *Cancer Res*
7 **1985**;45(5):2110-5.
- 8 34. Behrens BC, Hamilton TC, Masuda H, Grotzinger KR, Whang-Peng J, Louie KG, *et al.*
9 Characterization of a cis-diamminedichloroplatinum(II)-resistant human ovarian cancer
10 cell line and its use in evaluation of platinum analogues. *Cancer Res* **1987**;47(2):414-8.
- 11 35. Langdon SP, Lawrie SS, Hay FG, Hawkes MM, McDonald A, Hayward IP, *et al.*
12 Characterization and properties of nine human ovarian adenocarcinoma cell lines. *Cancer*
13 *Res* **1988**;48(21):6166-72.
- 14 36. Analysis of Drug Resistant Properties of A2780 Ovarian Cancer Cell Lines Using Label-
15 Free Automated Microscopy (IncuCyte ZOOM) Public Health England 2016.
- 16 37. Gottesman MM, Fojo T, Bates SE. Multidrug resistance in cancer: role of ATP-dependent
17 transporters. *Nat Rev Cancer* **2002**;2:48.
- 18 38. Ho Y-P, Au-Yeung SCF, To KKW. Platinum-based anticancer agents: Innovative design
19 strategies and biological perspectives. *Med Res Rev* **2003**;23(5):633-55.
- 20 39. Witney TH, Kettunen MI, Hu De, Gallagher FA, Bohndiek SE, Napolitano R, *et al.*
21 Detecting treatment response in a model of human breast adenocarcinoma using
22 hyperpolarised [1-¹³C]pyruvate and [1,4-¹³C₂]fumarate. *Br J Cancer* **2010**;103:1400.
- 23 40. Witney TH, Hoehne A, Reeves R, Ilovich O, Namavari M, Shen B, *et al.* A systematic
24 comparison of ¹⁸F-C-SNAT to established radiotracer imaging agents for the detection of
25 tumor response to treatment. *Clin Cancer Res* **2015**.
- 26 41. Witney TH, Fortt RR, Aboagye EO. Preclinical Assessment of Carboplatin Treatment
27 Efficacy in Lung Cancer by ¹⁸F-ICMT-11-Positron Emission Tomography. *PLOS ONE*
28 **2014**;9(3):e91694.
- 29 42. Alam IS, Neves AA, Witney TH, Boren J, Brindle KM. Comparison of the C2A Domain
30 of Synaptotagmin-I and Annexin-V As Probes for Detecting Cell Death. *Bioconjugate*
31 *Chem* **2010**;21(5):884-91.

- 1 43. Palmieri L, Elvas F, Vangestel C, Pak K, Gray B, Stroobants S, *et al.* [(99m)Tc]duramycin
2 for cell death imaging: Impact of kit formulation, purification and species difference. Nucl
3 Med Biol **2018**;56:1-9.
- 4 44. Lauber K, Ernst A, Orth M, Herrmann M, Belka C. Dying cell clearance and its impact on
5 the outcome of tumor radiotherapy. Front Oncol **2012**;2:116.
- 6 45. Ballatori N, Krance SM, Notenboom S, Shi S, Tieu K, Hammond CL. Glutathione
7 dysregulation and the etiology and progression of human diseases. J Biol Chem
8 **2009**;390(3):191-214.
- 9 46. Godwin AK, Meister A, O'Dwyer PJ, Huang CS, Hamilton TC, Anderson ME. High
10 resistance to cisplatin in human ovarian cancer cell lines is associated with marked increase
11 of glutathione synthesis. Proc Natl Acad Sci **1992**;89(7):3070-4.
- 12 47. Meijer C, Mulder NH, Timmer-Bosscha H, Sluiter WJ, Meersma GJ, de Vries EGE.
13 Relationship of Cellular Glutathione to the Cytotoxicity and Resistance of Seven Platinum
14 Compounds. Cancer Res **1992**;52(24):6885-9.
- 15 48. Bannai S, Ishii T. A novel function of glutamine in cell culture: utilization of glutamine for
16 the uptake of cystine in human fibroblasts. J Cell Physiol **1988**;137(2):360-6.
- 17 49. Perez RP, Hamilton TC, Ozols RF, Young RC. Mechanisms and modulation of resistance
18 to chemotherapy in ovarian cancer. Cancer **1993**;71(S4):1571-80.
- 19 50. Rabik CA, Dolan ME. Molecular Mechanisms of Resistance and Toxicity Associated with
20 Platinating Agents. Cancer treat rev **2007**;33(1):9-23.

21

22

23

24

25

26

1 **Figure Legends**

2 **Fig. 1. Chemotherapy resistance accompanies protection against oxidative stress in human**
3 **ovarian cell lines.** Sensitivity of A2780 (A and B) and PEO cell lines (C) to treatment with
4 cisplatin (A and C) or Doxil (B), as measured by an MTT assay. Data is expressed as a percentage
5 response compared to untreated cells following 72 h treatment ($n = 3$). (D and E) Global levels of
6 intracellular ROS in A2780 (D) and PEO (E) ovarian cancer cell lines, measured by flow
7 cytometry. Different laser power was used for data acquisition of A2780 matched lines vs PEO.
8 (F and G) Intracellular baseline GSH levels in the drug sensitive and drug resistance A2780 (F)
9 and PEO cell lines (G). Scatter plots represent individual biological repeats. *, $P < 0.05$; **, $P <$
10 0.01 ; ***, $P < 0.001$.

11

12 **Fig 2. [^{18}F]FSPG uptake is decreased in drug-resistant cells.** (A) Molecular structure of
13 [^{18}F]FSPG. (B and C) [^{18}F]FSPG cell uptake and accumulation following 60 min incubation in
14 A2780 cell lines (B) and PEO cell lines (C). Scatter plots represent biological repeats performed
15 in triplicate. *, $P < 0.05$; **, $P < 0.01$; ***, $P < 0.001$, ****, $P < 0.0001$.

16

17 **Fig. 3. Intracellular levels of cystine are decreased in drug-resistant cancer cells.** (A) Model
18 of [^{18}F]FSPG accumulation, with mechanisms known to control radiotracer accumulation. Uptake
19 of [^{18}F]FSPG is predicted to occur through exchange with intracellular glutamate, with efflux
20 controlled by the exchange with extracellular cystine. Red and green triangles represent the

1 concentration gradients of cystine and glutamate across the plasma membrane. e, extracellular; i,
2 intracellular. (B) Western blot analysis of the levels of xCT, glutaminase isozymes (kidney-type
3 glutaminase (KGA) and glutaminase-C (GAC)), glutamate-cysteine ligase (GCL) and NRF2.
4 Intracellular levels of glutamate (C and D) and cystine (E and F) in A2780 (C and E) and PEO
5 human ovarian cancer cell lines (D and F). Data presented as mean with individual scatter plots
6 representing independent experiments. *, $P < 0.05$; **, $P < 0.01$.

7

8 **Fig. 4. [¹⁸F]FSPG uptake is decreased in Doxil-resistant A2780 tumors** (A) Representative
9 PET/CT maximum intensity projections in WT and DoxR tumor-bearing mice 40-60 min post-
10 injection. White arrowheads indicate the tumor margins. (B) Quantification of [¹⁸F]FSPG tumor
11 uptake. Total GSH (C) and the ratio of GSSG:GSH (D) in *ex vivo* tumor samples. ***, $P < 0.001$.
12 Scatter plots represent tumors from separate mice. (D) Western blot analysis evaluating the
13 expression of proteins involved in cellular antioxidant response and proteins that may influence
14 [¹⁸F]FSPG uptake ($n = 3$ xenografts per tumor cell line). Actin was used as a loading control. KGA,
15 kidney-type glutaminase; GAC, glutaminase-C; GCL, glutamate-cysteine ligase.

16

17 **Fig. 5. [¹⁸F]FSPG uptake is unchanged in A2780 DoxR tumors that fail to respond to therapy.**
18 (A) The treatment and imaging protocol. (B) Representative PET/CT maximum intensity
19 projections in chemotherapy resistant A2780 DoxR tumor-bearing mice prior to treatment (D0) or
20 following either 24 h (D1) or 6 days of Doxil treatment (D6). SG, salivary glands. (C)
21 Quantification of tumor uptake in all three treatment groups ($p > 0.05$). (D) A2780 DoxR tumor

1 growth curves in untreated and drug-treated mice ($p > 0.05$). Total intracellular GSH concentration
2 (E) and GSSG:GSH ratio (F) from tumor samples taken from untreated and Doxil-treated mice
3 taken immediately following PET imaging ($p > 0.05$). Scatter plots represent tumors from separate
4 mice. (G) Expression of apoptotic cell death and oxidative stress protein markers. Actin was used
5 as a loading control. Prolonged exposure relates to a 45 min exposure using a cleaved caspase 3
6 primary antibody.

7

8 **Fig. 6. Schematic illustrating the proposed mechanism of [^{18}F]FSPG accumulation in**
9 **sensitive and drug-resistant tumors.** Changes in the concentration gradients of either cystine or
10 glutamate in drug resistant (A) and drug sensitive (B) tumor cells are predicted to cause alterations
11 in [^{18}F]FSPG tumor retention. A decrease in intracellular cystine leads to an increase in the
12 concentration gradient across the membrane, expected to result in increased efflux of [^{18}F]FSPG
13 in exchange for more extracellular cystine. Alternatively, decreased uptake in drug-resistant
14 tumors may be a consequence of increased competition between cystine and [^{18}F]FSPG at the site
15 of the transporter (denoted by the yellow star). Red and green triangles represent the concentration
16 gradients of cystine and glutamate, respectively. e, extracellular; i, intracellular.

17

18

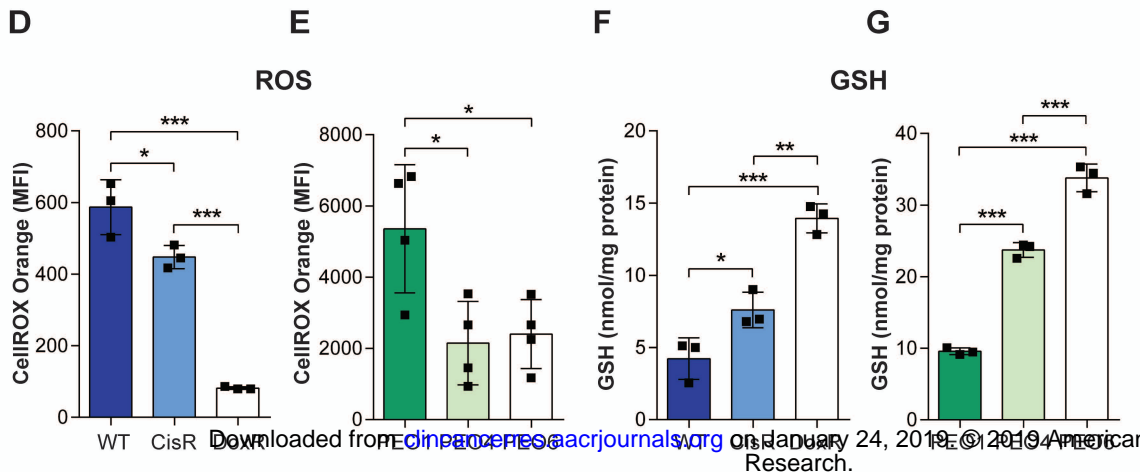
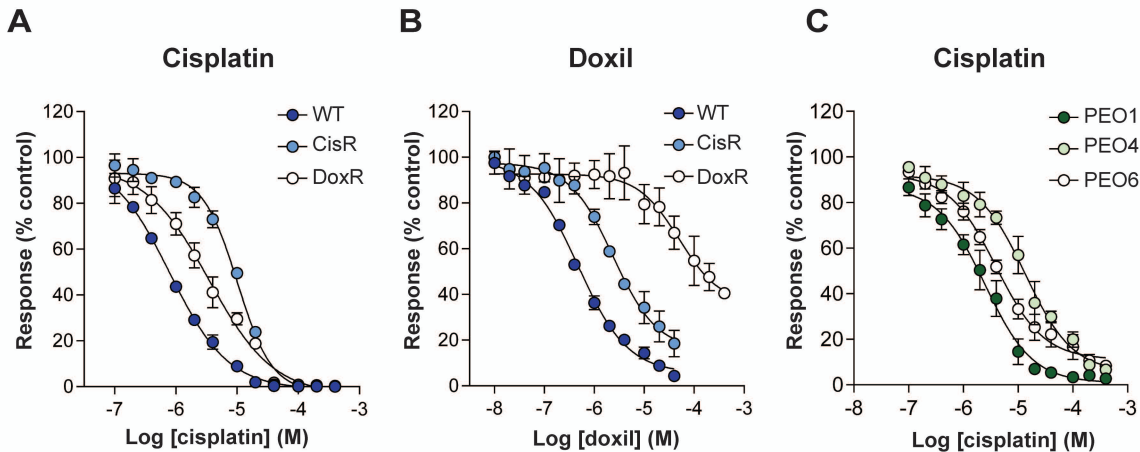
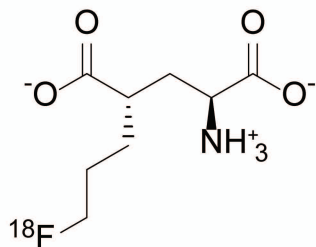
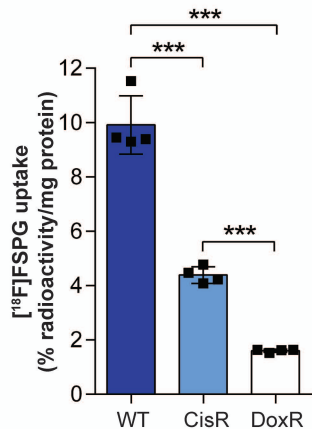
Figure 1

Figure 2

A



B



C

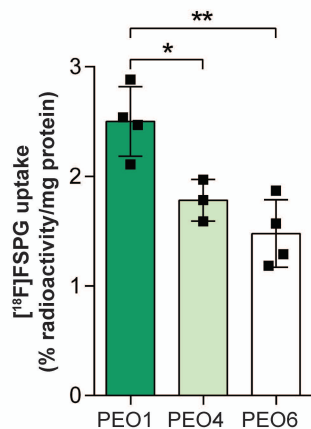


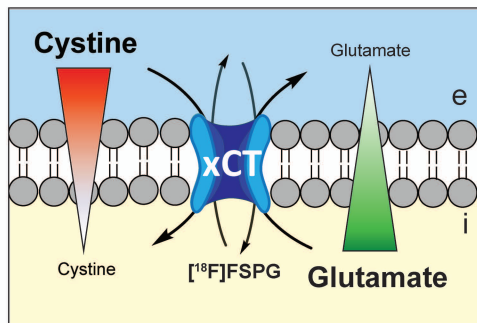
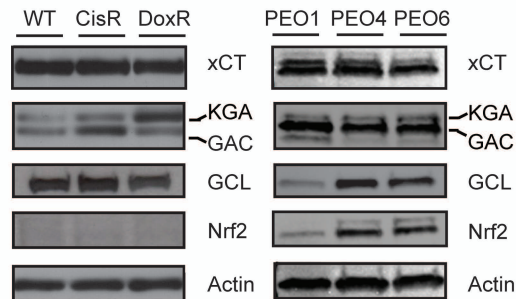
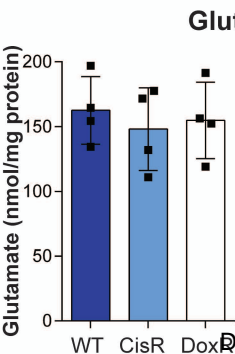
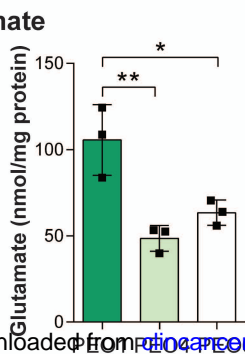
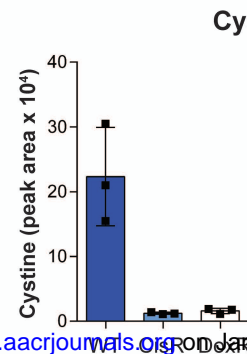
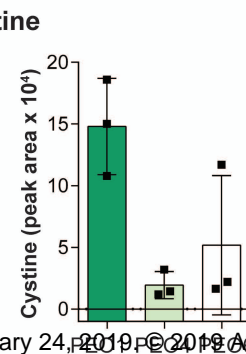
Figure 3**A****B****C****D****E****F**

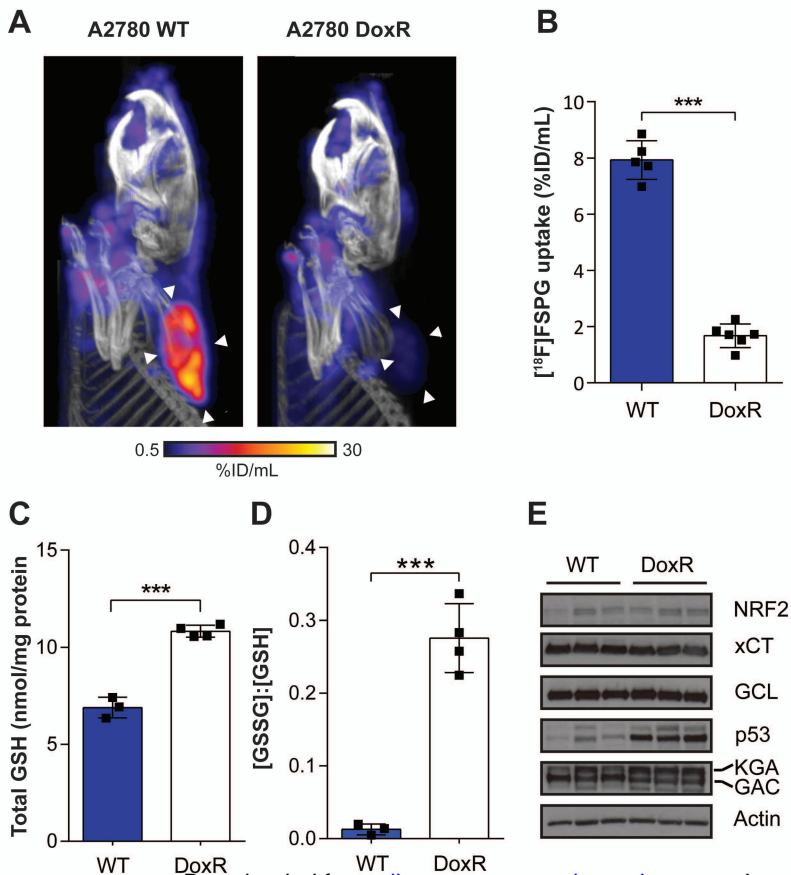
Figure 4

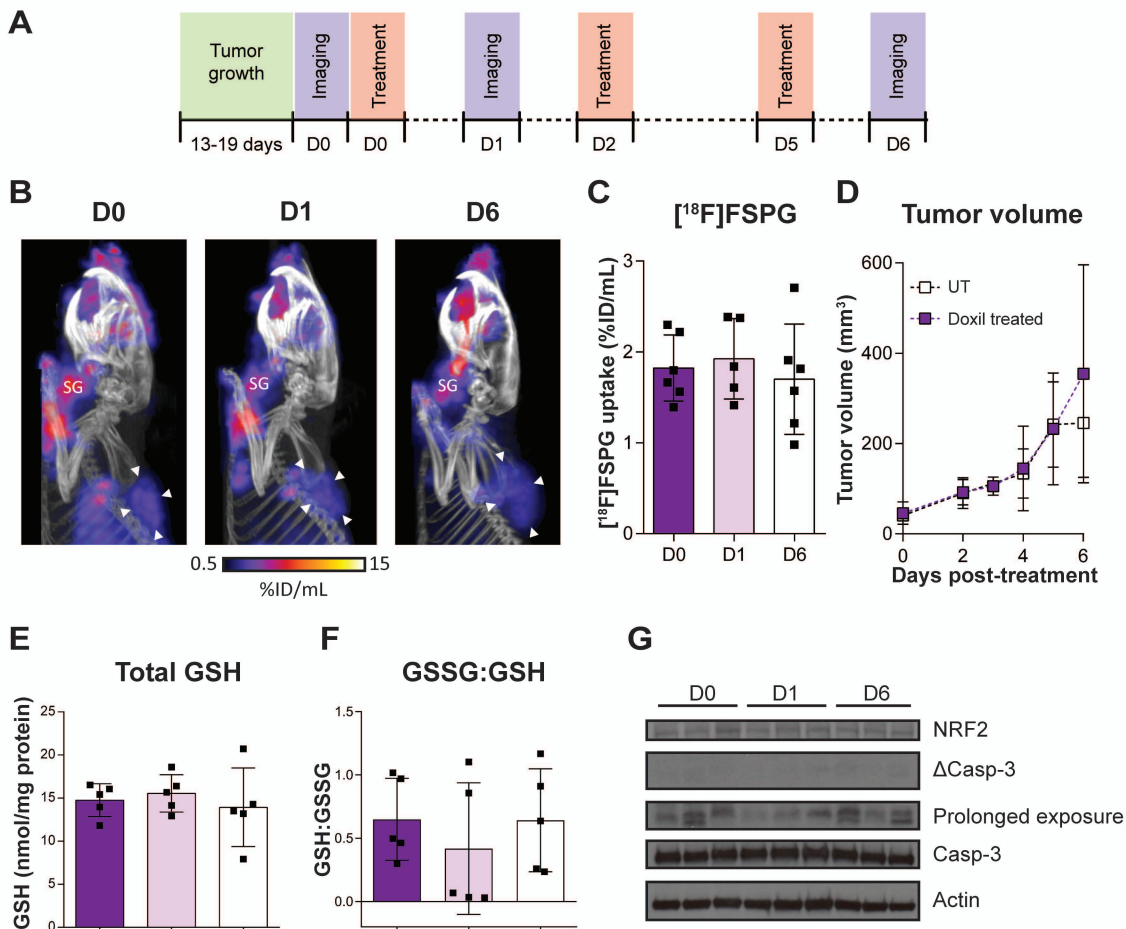
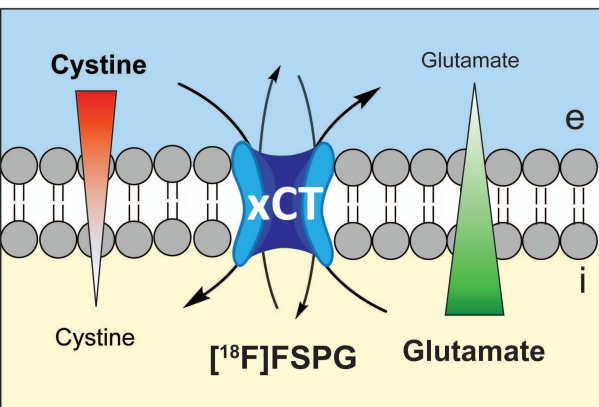
Figure 5

Figure 6

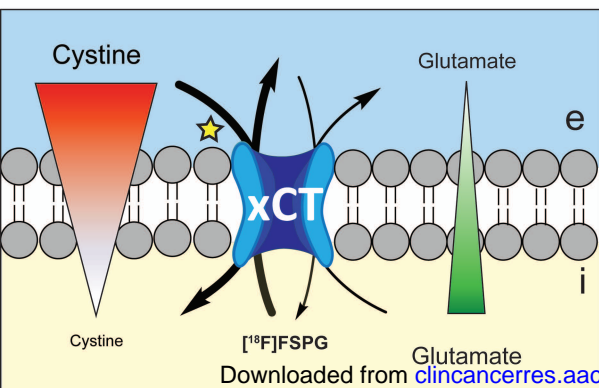
A

Drug-sensitive



B

Drug-resistant



Clinical Cancer Research

Measurement of tumor antioxidant capacity and prediction of chemotherapy resistance in preclinical models of ovarian cancer by positron emission tomography

Hannah E Greenwood, Patrick N McCormick, Thibault Gendron, et al.

Clin Cancer Res Published OnlineFirst January 16, 2019.

Updated version	Access the most recent version of this article at: doi: 10.1158/1078-0432.CCR-18-3423
Supplementary Material	Access the most recent supplemental material at: http://clincancerres.aacrjournals.org/content/suppl/2019/01/16/1078-0432.CCR-18-3423.DC1
Author Manuscript	Author manuscripts have been peer reviewed and accepted for publication but have not yet been edited.

E-mail alerts	Sign up to receive free email-alerts related to this article or journal.
Reprints and Subscriptions	To order reprints of this article or to subscribe to the journal, contact the AACR Publications Department at pubs@aacr.org .
Permissions	To request permission to re-use all or part of this article, use this link http://clincancerres.aacrjournals.org/content/early/2019/01/16/1078-0432.CCR-18-3423 . Click on "Request Permissions" which will take you to the Copyright Clearance Center's (CCC) Rightslink site.